Chapter 4

The Formation of Photonic Band Gap in a Two-dimensional Square Lattice of Dielectric Rods in Air

It is well known that the most severe limit to the PBG width comes from the degeneracy of photonic bands at high symmetry point in the Brillouin zone. Several methods have been suggested for lifting the band degeneracy and obtaining the complete PBG, which involve varying the contrast of dielectric contrast ratio, design of lattice element, filling ratio and reducing the structural symmetries. Generally, the PCs have been mainly investigated for square, hexagonal and triangular lattices of air rods or dielectric rods with various cross sections. In the chapter 3, we have shown that the complete PBG for square lattice appears when the rods are designed with dielectric square columns, whereas closes when the rods are designed with circular cross section of the columns. This is an interesting issue that the isolated-dielectric rods can appear an complete PBG by the use of square rod without including dielectric veins. The regular shape and the side of dielectric rods may strong affect the band structures in the square lattice. Hence, in order to understand this issue, we increase the symmetry of rod up to circular rod in this work. Now, we consider the 2D photonic crystals with dielectric N-polygonal rods as inclusions in the square lattice. The plane-wave method is employed in this study to calculate the band structures and field patterns. The effects of N-polygonal rods on the E-polarization and H-polarization band structures have been examined. Our calculations also show that the band

structures of polygonal rod approach the same to that of circular rod while N is large. These results may provide a guiding for fabricating the photonic crystals. Moreover, we have shown that the relative position for either E-polarization or H-polarization band gaps in the anisotropic PCs can be matched to obtain a large complete PBG. Following these ideas, we also calculate the band structures of N-polygonal rod with anisotropic materials, under the same filling factor, to find a large complete PBG in this photonic crystal.

Our calculations have also shown that the use of octagonal rods as inclusions in the square lattice can not open the complete PBG. It is interesting that there is such difference between square and octagonal rods in the square lattice. To understand how the boundary of rods affects the formation of PBG in square lattice, we little by little cut the corners of square rod to form octagonal shape at the fixed filling factor. The effect of the rods' shape on the E-polarization and H-polarization modes is examined. In particular, the band center and the band width of bands associated with the complete PBG of square dielectric rods in the square lattice have been calculated either. From the band-structure viewpoint, it provides a simple and helpful method to understand how the complete PBG disappears in the octagonal structure.

4.1. The Dielectric Function of Polygonal Structure

Assuming the dielectric material in the photonic crystal has an anisotropic refractive index; the principal refractive indices are the ordinary refractive index n_0 and the extraordinary refractive index n_e. The extraordinary axis is set to be parallel to the axis of the rod. The refractive index is n_e when the electric field vector in the E-polarization mode is parallel to the extraordinary axis, while the refractive index is

n_0 when the electric field vector in the H-polarization mode is perpendicular to the extraordinary axis. The calculations are restricted to the case in which the wave vectors of the eigenmodes lie in the 2D x-y plane and are uniform in the z-direction. The dielectric constant is given by

$$\varepsilon(\vec{r}) = \varepsilon_b + (\varepsilon_{e,o} - \varepsilon_b) \cdot S_{rod}(\vec{r}) \tag{4.1}$$

where $S_{rod}(\vec{r})$ is a function for the rod. Dielectric constants ε_e and ε_o respectively correspond to the refractive index n_e and n_0. The Fourier coefficient can be expressed as,

$$\varepsilon(\vec{G}) = \begin{cases} \varepsilon_{e,o} \cdot f + \varepsilon_b \cdot (1-f) & \text{for } \vec{G} = 0 \\ (\varepsilon_{e,o} - \varepsilon_b) \cdot S(\vec{G}) & \text{elsewhere} \end{cases} \tag{4.2}$$

The filling factor f is the cross-sectional area fraction in a primitive unit cell. The structure factor is denoted by $S(\vec{G}) = \frac{1}{A_{cell}} \int_{Rod} e^{-i\vec{G}\cdot\vec{r}} dr$. For the circular rod, the structure factor is given by

$$S(G) = \frac{2\pi r_a}{G} J_1(G r_a) \tag{4.3}$$

where $G = |\vec{G}|$ and J_1 is the first-order Bessel function of the first kind. r_a is the radius of circular rod. For the polygonal rod, we consider a polygonal rod with N sides, and the coordinate of jth vertex is denoted $\vec{P}_j = (x_j, y_j)$. According to Stokes' theorem, the structure factor for the polygonal rod can be written,

$$S(G) = \begin{cases} \sum_{j=1}^{N} \frac{i\Delta y_j e^{-i\vec{G}\cdot\vec{C}_j}}{G_x} \frac{\sin(\vec{G}\cdot\vec{S}_j)}{\vec{G}\cdot\vec{S}_j} & \text{for } G_y = 0 \\ \sum_{j=1}^{N} \frac{-i\Delta x_j e^{-i\vec{G}\cdot\vec{C}_j}}{G_y} \frac{\sin(\vec{G}\cdot\vec{S}_j)}{\vec{G}\cdot\vec{S}_j} & \text{for } G_x = 0 \\ \sum_{j=1}^{N} \frac{2i\hat{e}_z(\vec{G}\times\vec{S}_j) e^{-i\vec{G}\cdot\vec{C}_j}}{G^2} \frac{\sin(\vec{G}\cdot\vec{S}_j)}{\vec{G}\cdot\vec{S}_j} & \text{for } G_x \neq 0,\ G_y \neq 0 \end{cases} \tag{4.4}$$

where

$\vec{C}_j \equiv (\frac{\vec{p}_{j+1} + \vec{p}_j}{2})$, $\vec{S}_j \equiv (\frac{\vec{p}_{j+1} - \vec{p}_j}{2})$ and $\Delta x \equiv x_{j+1} - x_j$, $\Delta y \equiv y_{j+1} - y_j$.

The band structures for a photonic crystal are calculated by the standard plane-wave method. The calculations for anisotropic photonic crystals are calculated in the same way as for isotropic photonic crystals. In this study, 841 plane waves were adopted, and the computational errors in the E- and H-polarization modes for each case were estimated to be less than 1%.

4.2. Photonic Band Gap in a Two-dimensional Square Lattice of Polygonal Dielectric Rods in Air

Figures 4.1(a) and (b) show the size of side, the radii of inscribed circle (R-inner) and circumcircle (R-outer) in unit of lattice constant a for each equilateral polygon, respectively. In our study, each polygonal structure in Fig. 4.1 has the same filling factor. The optimal filling factor of square rods, taking as $f = 0.45$, is adopted throughout the simulations for either isotropic or anisotropic photonic crystals. The dielectric constant of rod is chosen as 12.96, which corresponds to that of GaAs or Silicon at 1.55 μm, and the dielectric constant for the background material is taken as air with $\varepsilon_b = 1$. Figures 4.2(a) and (b) show the photonic band structures associated with the circular rods $(N = \infty)$ and square rods $(N = 4)$ in the square lattice, respectively, at a filling factor of 0.45. The solid curves are for E-polarization modes and the dotted curves are for H-polarization modes. The dispersion curves have been traced along the T-X-M-T path in the first Brillouin zone of square lattice. As shown in Fig. 4.2(a), the circular rods in the square lattice do not open an enough size of H-polarization band gap when the frequency is less than 1.0 $(\omega a / 2\pi c)$. The results consequently show the absence of complete PBG in this photonic structure. On the

other hand, the calculated band structures of square rods are shown in Fig. 4.2(b), with a sizable complete PBG at high normalized frequencies (about 0.62) of EM waves. The complete PBG occurs in E_8 and H_6 gaps overlap, where E_i and H_i denote the gap that appears between the i_{th} and $(i+1)_{th}$ bands for the corresponding polarizations.

Figure 4.3 presents the dependence of gap width of each polarization mode on number of side (N) of equilateral polygon. Here we only consider the bands below fourteenth band for both polarizations. As the results, the shape of polygonal rods influences gap width slightly as N is even, whereas that influences gaps strongly as N is odd. Moreover, because the H-polarization gap width can not be widened and overlapped with E-polarization gap width on increasing N, so no complete PBG presents.

The fields for H polarization are oriented in the x-y plane and the tangential fields that link nearest-dielectric rods must be forced to penetrate into low dielectric background regions (air) to satisfy the continuity boundary condition. The electromagnetic interaction between high-dielectric rods affects the proportion of field energy in the dielectric regions, and thereby changes the band structures of H-polarization modes. As shown in the Fig. 4.1(b), the radius of circumcircle decreases as N increases. The air-space size among the nearest-dielectric rods is small for small N, indicating that the wave scattering among rods affects the H-polarization bands drastically, strongly varying the H-polarization band gaps. When N is greater than ten, the air-space size remains almost constant, and varies below 1% with varying N. This means that the interaction between the fields of the rods affects the H-polarization bands in almost the same way, slightly changing the H-polarization band gap. The gap-midgap ratio is the ratio $r \equiv \Delta\omega/\omega_0$ of the gap

width $\Delta\omega = \omega_U - \omega_D$ to the midgap frequency ω_0, where ω_D and ω_U are the lower and upper band corner frequencies of the gap, respectively. The ratio of H-polarization gap of circular structure is $r = 4.5\%$. The difference in gap-midgap ratio between the circular and polygonal structures there is less than 1% as N is greater than ten.

In the E-polarization mode, the proportion of field energy concentrated in the dielectric regions dominates the gap width and band frequency. The field patterns for each structure are examined to investigate the effect of polygonal structure on the E-polarization modes. Figures 4.4(a)-(h) show the field patterns of structures from N=4 to N=11, respectively. Figure 4.4(i) shows those for circular structure. The E-polarization mode is associated with the displacement field D normal to the plane, $D(\vec{r}) = d(\vec{r})\hat{e}_z$, where $d(\vec{r})$ is a scalar function. The field patterns in each figure are displayed for the E_8 band at the *M*-symmetry point. It is obviously that the field energies can be localized inside the dielectric rods for even N and circular structures. The result is reasonable to suppose that the E-polarization bands for even N structures are quite similar to circular structure. However, the fields for odd N structures can not be confined well in the dielectric regions, N=5 especially. Partial fields inside the rods are expelled out from the dielectric regions. This reflects that the E-polarization bands in the pentagonal structure tend to move toward higher normalized frequencies in comparison with N=4. Furthermore, the amplitude of the displacement field, the field distribution and the amount of field energy in the dielectric regions are almost the same with those in Fig. 4.4(f) when N is increased. The E_8 gap of circular structure is a gap-midgap ratio of 14.8%. The difference in gap-midgap ratio between circular and polygonal structures is less than 1% as N is greater than twelve.

From the above discussions in E-polarization and H-polarization modes, the

number of side of polygonal rods in the square lattice is not favorable for affecting the band structures as N is greater than twelve. These results may provide guidance for designing and fabricating polygonal structure in the square lattice. Moreover, the band structures N=12 with filling factor f=0.45 are plotted in Fig. 4.5. The band-structure features for both polarizations are identical with that in Fig. 4.2(a).

Next, we calculated the photonic band structures of polygonal and circular structures with tellurium (Te) rods. The refractive indices of Te are assumed as constants and the absorption effect is neglected in our calculations. Figure 4.6(a) and (b) show the photonic band structures for a square lattice of anisotropic circular and square rods in air, respectively, at a filling factor of 0.45. The circular rods with anisotropic material appear two large complete PBG, but the square rods with anisotropic material close the complete PBG. The dependence of gap map on number of side N of polygonal structure is displayed in Fig. 4.7. Because the refractive indices for both polarizations are increased simultaneously, the overall bands of either E-polarization or H-polarization modes tend to move toward lower frequencies in comparison with that in Fig. 4.3. In particular, the H-polarization gap opens a sizable width for each N, and overlaps well with E-polarization gaps. Hence, the large complete PBGs appear in photonic crystals when the polygonal rods are designed with anisotropic materials.

The difference in H-polarization gap-midgap ratio between circular and polygonal structures is less than 1% for $N \geq 10$. The features of H-polarization bands on varying N can be understood by using the same qualitative arguments as for isotropic cases. However, the E-polarization bands of anisotropic structure are more sensitive to N than that of isotropic structure. The gap-midgap ratio of E_3 gap of circular structure is 17.5%. The difference between N-polygonal structures and circular

structure is less than 1% as N is greater than eighteen. It is obviously that the band structures strongly depend on the shape and the boundary of polygonal rods if the photonic crystals are designed with an anisotropic material as inclusions. For this reason, the fabrication requirements of anisotropic photonic crystal should be more precise than that of isotropic photonic crystal.

4.3. Photonic Band Gap in a Two-dimensional Square Lattice of Corner-cutting Dielectric Rods in Air

Figure 4.8 shows the representation and the cross-sectional geometry of the rods. The sizes of cutting corner and rod's side are defined as b and ℓ, respectively. Each corner-cutting structure has the same filling factor of the dielectric rod $f = 0.45$. The difference in the size of cutting corner between square and octagonal rods is $a \cdot \ell_8 / \sqrt{2}$, where ℓ_8 is the size of side of the octagonal rod and a is the lattice constant of square lattice. In this work, the corner-cutting calculations from square to form octagonal shapes are divided into fifteen equal parts, and the increment is defined as $\beta = a \cdot \ell_8 / (15 \cdot \sqrt{2})$. For convenience, we describe the size of cutting corner as $b = m \cdot \beta$, where $m = 0,1,\cdots 14,15$.

Figures 4.9 show the photonic band structures of octagonal rods ($b = 15 \cdot \beta$) in the square lattice, at a filling factor of 0.45. The band structures of the square rods ($b = 0 \cdot \beta$) in the square lattice have shown in Fig. 4.2(b). The square dielectric rods in the square lattice appear a complete PBG occurring in E_8 and H_6 gaps overlap, the complete gap center is 0.628 ($\omega a / 2\pi c$) and the complete PBG width is 0.036 ($\omega a / 2\pi c$). Contrary the Fig. 4.9 shows that the complete PBG is closed when the square dielectric rods are replaced with the octagonal dielectric rods. It is

suggested that four corners of square rods may have a strong influence on the band structure.

To understand why there is such difference in appearance of complete PBG between square rod and octagonal rods in the square lattice, we little by little cut the corners of square rods to form octagonal shape at the fixed filling factor. Figure 4.10 shows the dependence of the gap map on *m*. Here we only consider the frequency range of interest from 0.55 to 0.7 ($\omega a/2\pi c$). As the results, the widths for both E_8 and H_6 gaps simultaneously decline as *m* increases. The variation in the frequencies of air bands (E_9 and H_7 bands) is larger that those of dielectric bands ($E_8$and H_6 bands), and drastically reduces the complete gap width.

The field patterns for structures of *m*=0, 8, 11 and 15 are plotted in Figs. 4.11(a)-(d) respectively, to examine the effect of cutting corner on the E-polarization modes. The field patterns of each figure are displayed for E_8 (left part) and E_9 (right part) bands at the *M*-symmetry point. The field distributions of E_8 band are almost independent of *m*, but the amounts of field energy inside the rods increase as *m* increases. For the field patterns of E_9 band, it is obviously that the shape of rods strongly affects the field distribution and the amount field energy. When *m* increases, the fields near the boundary of rod are expelled out from the dielectric regions and the amounts of field energy are decreased. Because the amount of field energy inside the dielectric rods has strong related to the frequency of band, the difference in the amounts of field energy between E8 and E9 bands leads to the absence of E-polarization gap.

Following we use the band-structure viewpoint to understand why the complete PBG appear in the square rods, but close in the octagonal rods. For a given band, the band center (BC) reflects the resonant frequency of modes, while the band width (BW) reflects the strength of the interaction of electromagnetic waves among rods. These

band-structure concepts are similar to those in the LCAO method. Here the BC and BW are defined as,

$$F_i(BC) = \frac{F_{i,\max} + F_{i,\min}}{2} \qquad \text{and} \qquad F_i(BW) = F_{i,\max} - F_{i,\min} \tag{4.5}$$

where $F_{i,\max}$ and $F_{i,\min}$ respectively denote the maximum and minimum frequencies of i_{th} band in the first Brillouin zone. Here the E-polarization and H-polarization bands associated with the complete PBG in the photonic crystal are chosen. Figure 4.12(a) and (b) respectively show the band center and band width of E_8 and E_9 bands as a function of *m*. The BC of E_9 band varies more than that of E_8 band when *m* exceeds four. These results reflect that the effect of cutting corner on the resonance frequency of E_9 band is stronger than that of E_8 band, and the resonance frequencies for both bands approach gradually as *m* increases. Furthermore, we turn to examine BW to study how field energy concentrates inside dielectric regions to influence the band structures. The BW of E_9 band on increasing *m* is much different to that of E_8 band. The BW for the E8 band is almost independent of *m*, and may imply that the field energies are strongly localized in the dielectric rods. However, the BW of E_9 band reveals a large variation and increases to 137% at *m* =11. The results may reflect that partial fields of E_9 band are expelled out from the dielectric rods when the cutting corner of the rod is changed. Although the BC and BW of E_8 band are insensitive on shape or boundary of the rods, the decrease in BC and the increase in BW for the E_9 band lead to close the E-polarization gap when *m* exceeds eleven. The results and discussions with the band-structure viewpoint are similar to that with the field patterns, and it may provide a simple and effective method to understand the features of the band structures.

Figures 4.13(a) and (b) show the band center and band width associated with the H_6 and H_7 bands for various *m*. The BC of H_6 band varies slightly with *m*, but the BC of

H_7 band varies markedly. It indicates that the resonance frequency of H_7 band strongly depends on the shape of the rod. Moreover, the BWs for both H_6 and H_7 bands reveal a large variation with *m* and all increase about 0.017 as *m* is eleven. These mean that the fields propagated in the x-y plane can not be well-localized inside the dielectric region when cutting corner of the rod is changed. In fact, the fields of H-polarization modes concentrated in the rods are strong related to the air-pace size among the rods. This work assumes that the filling factor remains constant throughout calculations, and the air-space size among rods consequently varies with *m*. Therefore, it is reasonable to understand that both bands have the same increment of BW. Because of the decrease in resonance frequency of H_7 band and the increase in band widths for both H_6 and H_7 bands, the H-polarization gap is closed.

In this chapter, we investigate why the complete PBG appear in the square lattice when the square dielectric rods are used, but closes for circular or polygonal dielectric rods. The features for both E- and H-polarization bands are examined from the band-structure and the field-pattern perspectives. Polygonal structure and corner-cutting structure are considered in this chapter. The photonic crystals of anisotropic polygonal rod obtain a larger complete PBG width than that of isotropic polygonal rod. The band structures of isotropic rods approach the same as that of circular rod for N is greater than twelve, while that of anisotropic rods resemble to circular rods for N is greater eighteen. The E-polarization bands of anisotropic photonic crystal are more sensitive to rods' boundary than that of isotropic structure, and the fabrication requirements of anisotropic photonic crystal consequently are more stringent than that of isotropic photonic crystal. These results may provide a guiding for designing and fabricating the N-polygonal structure in the square lattice.

For the corner-cutting structures, the field patterns and band-structure viewpoints are used to understand the features of formed PBG in the square lattice. The results

in the E-polarization gap (E_8 gap) reveal that the cutting corner of rods strongly affects the E_9 band in resonance frequency and field distribution inside the rod. The decrease in resonance frequency and the increase in band width lead to close the E-polarization gap. The results in the H-polarization gap (H_6 gap) reveal a strong relationship between cutting corner of the rod and the H_6 or H_7 bands. The decrease in resonance frequency of H_7 band and the increase in band widths for both H_6 and H_7 bands lead to close the H-polarization gap. Accordingly, the complete PBG is closed in the square lattice when the square dielectric rods are replaced with the octagonal dielectric rods. The band-structure viewpoint is a simple and effective method, and is helpful in understanding the formation of PBG in the photonic crystal.

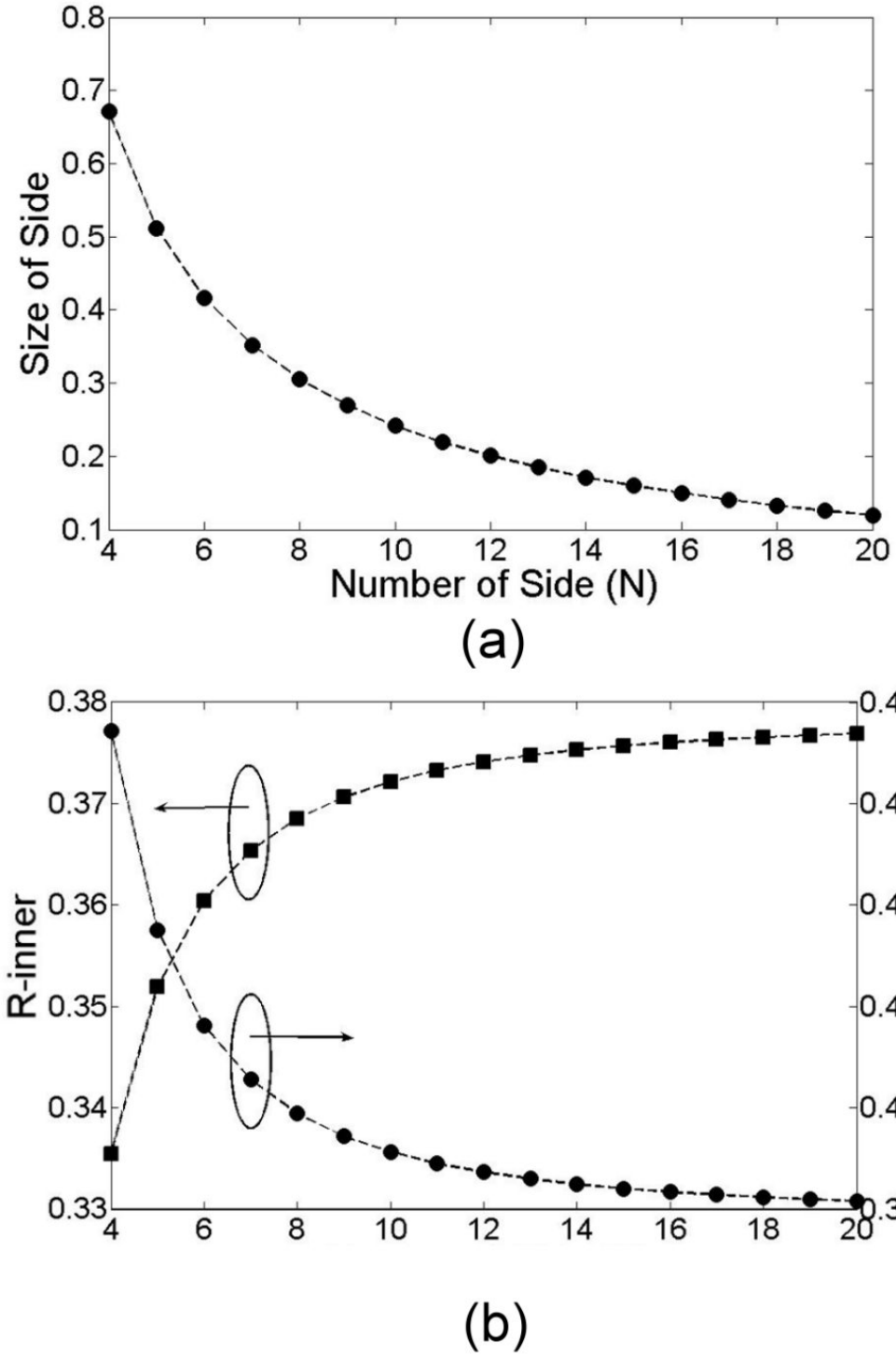

Figure 4.1 (a) the size of side, and (b) the radius of inscribed circle and circumcircle, corresponds to each equilateral polygon with a filling factor of 0.45.

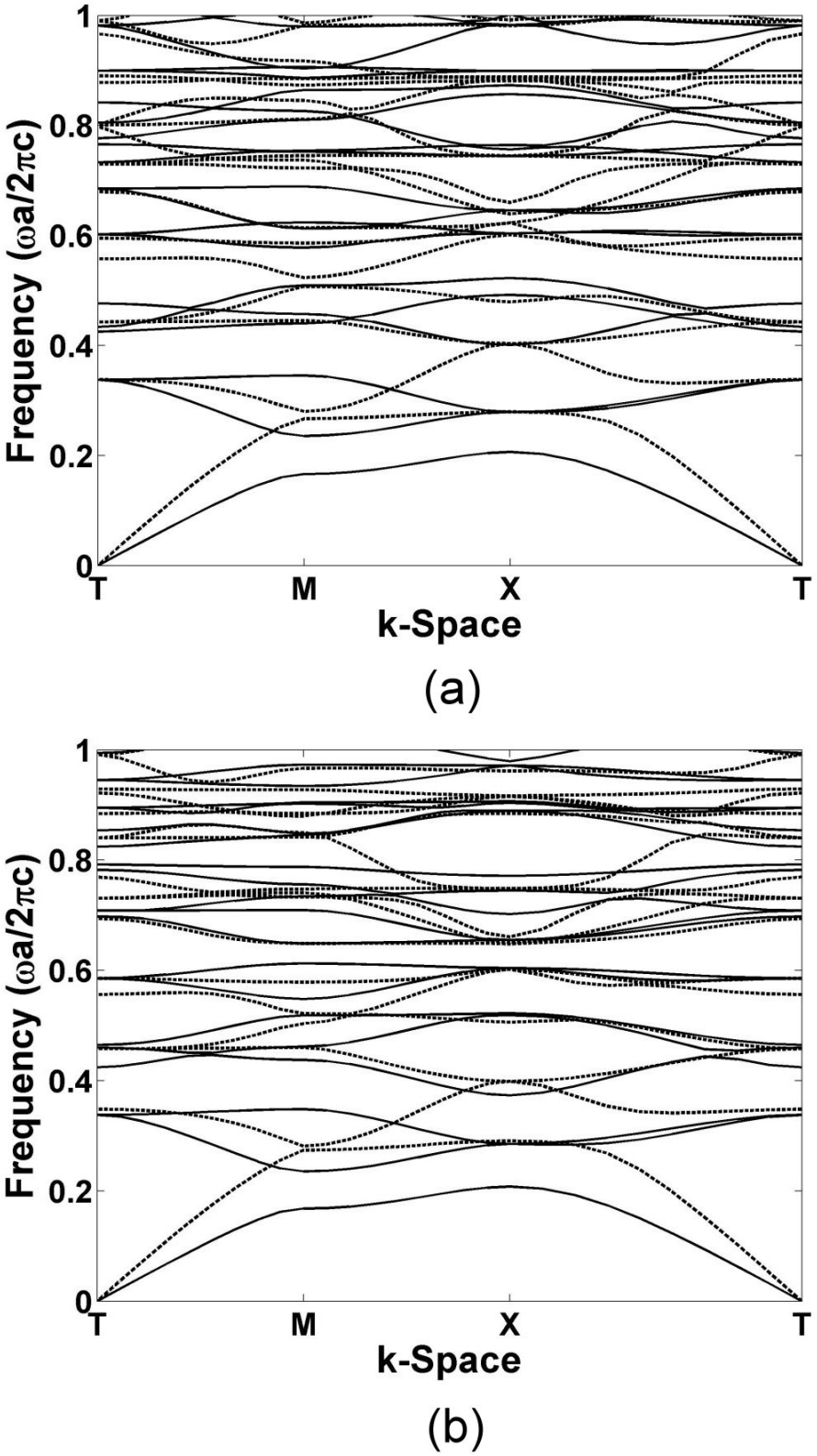

Figure 4.2 The photonic band structures associated with (a) circular rods and (b) square rods in the square lattice, at a filling factor of 0.45.

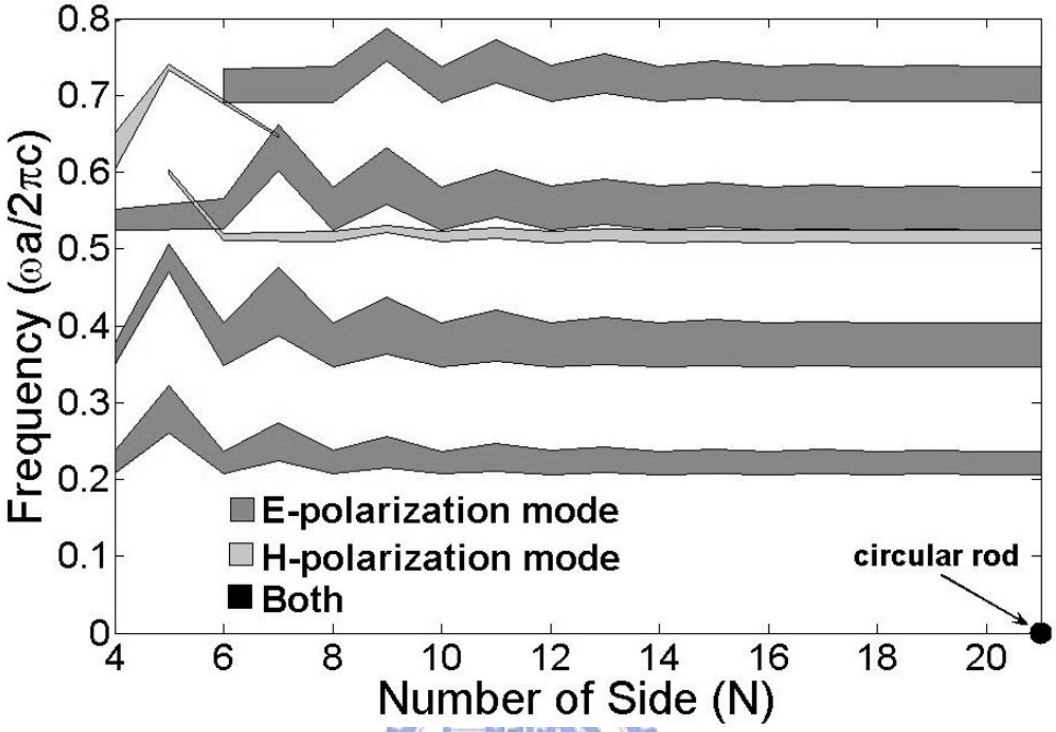

Figure 4.3 Gap width as a function of number of side N of equilateral polygon, at a filling factor of 0.45.

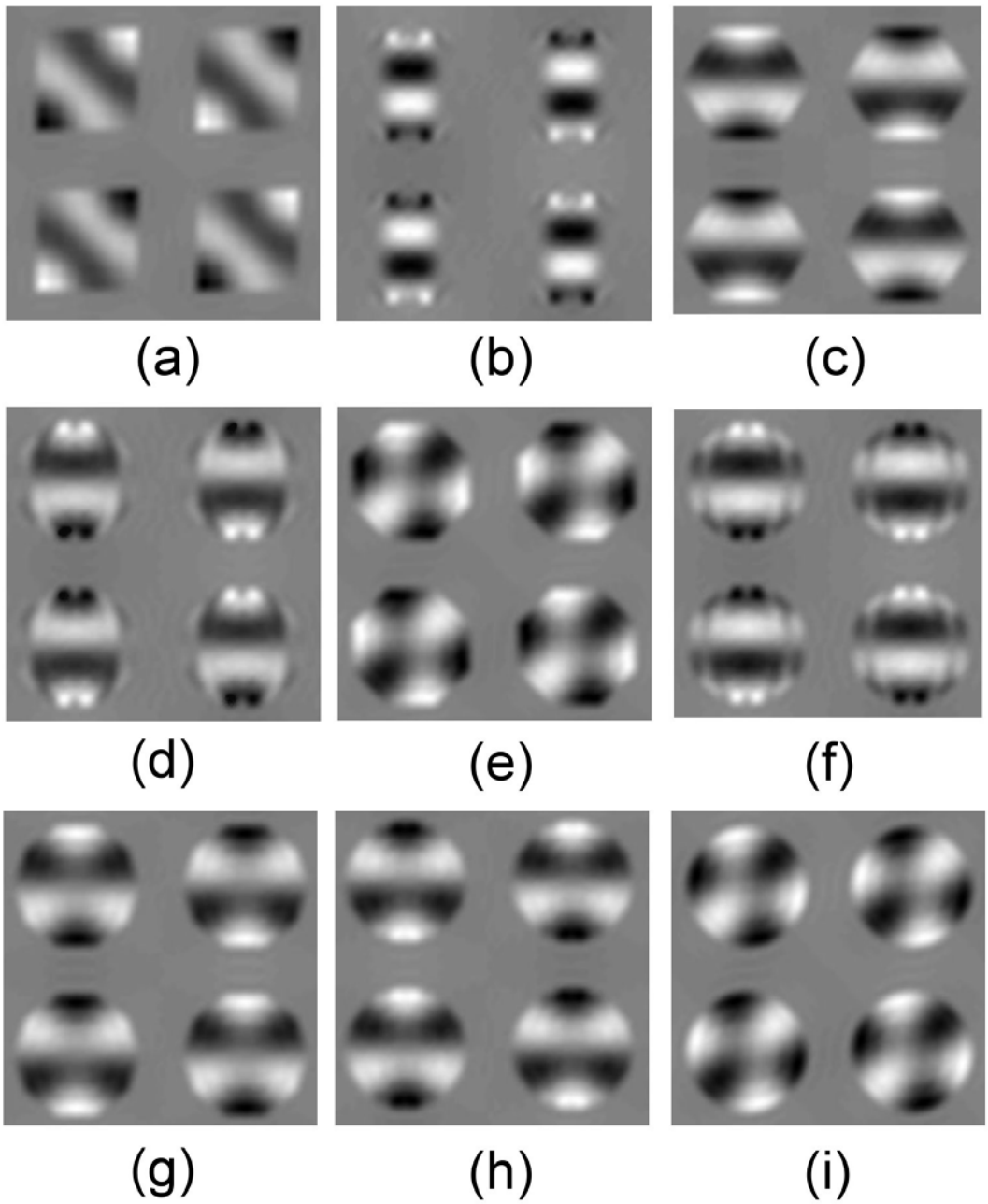

Figure 4.4 Field patterns of E-polarization modes inside polygonal rods of (a) N=4 (b) N=5 (c) N=6 (d) N=7 (e) N=8 (f) N=9 (g) N=10 (h) N=11 and (f) circular rod, for the E8 band and at the *M*-symmetry point.

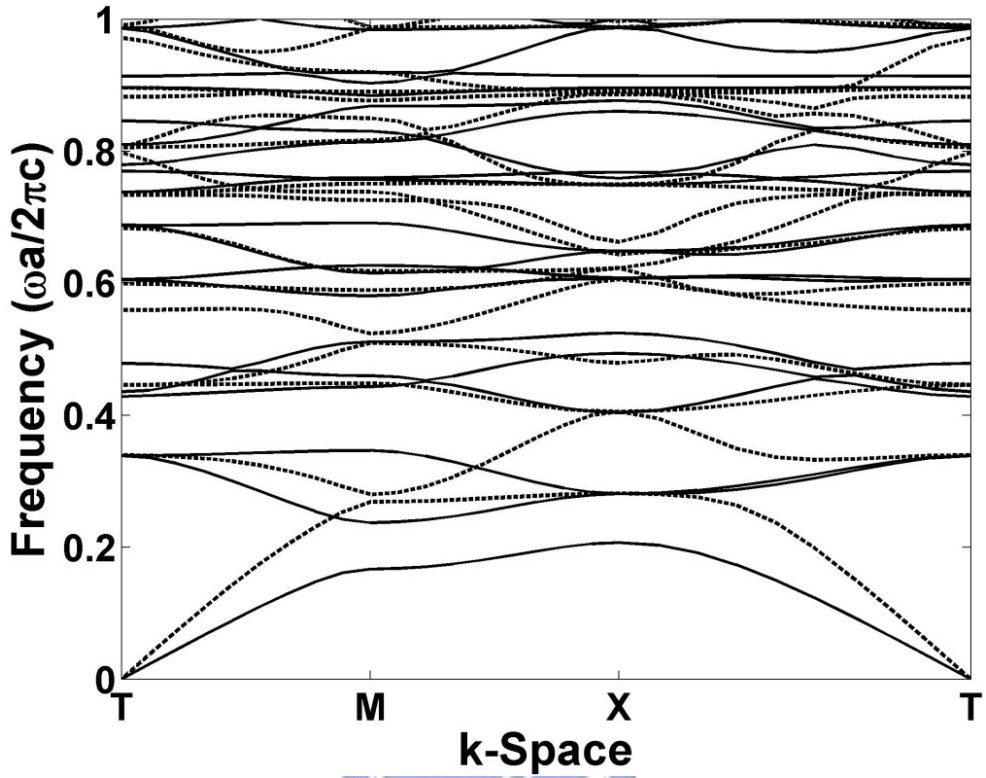

Figure 4.5 The photonic band structures of polygonal rod of N=12 in the square lattice, at a filling factor of 0.45.

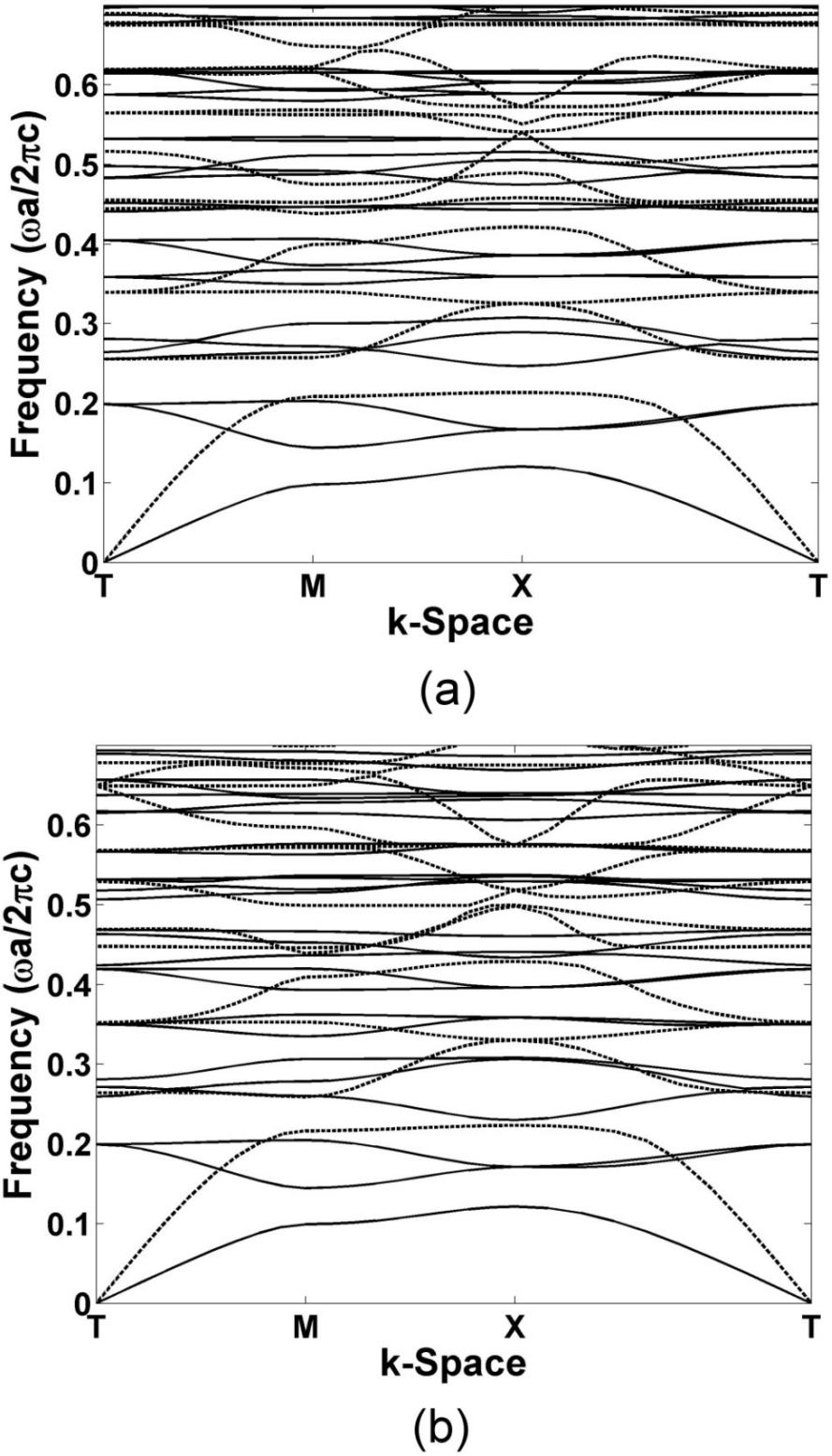

Figure 4.6 The photonic band structures for a square lattice of anisotropic (a) circular rods and (b) square rods in air, at a filling factor of 0.45.

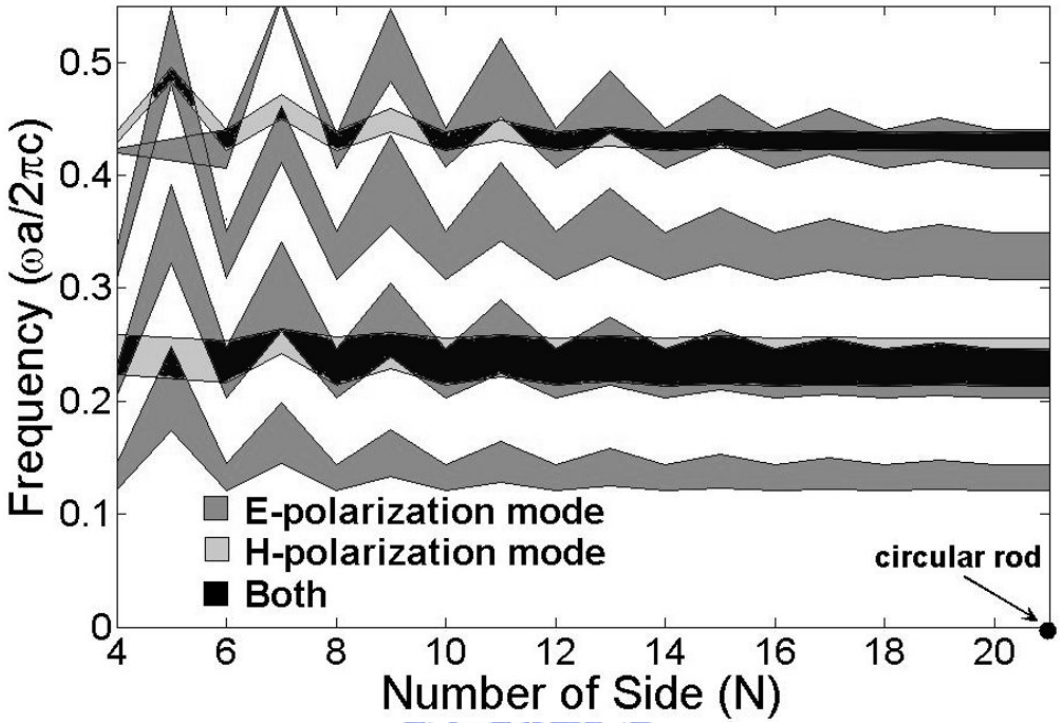

Figure 4.7 Gap width as a function of number of side N of equilateral polygon, at a filling factor of 0.45.

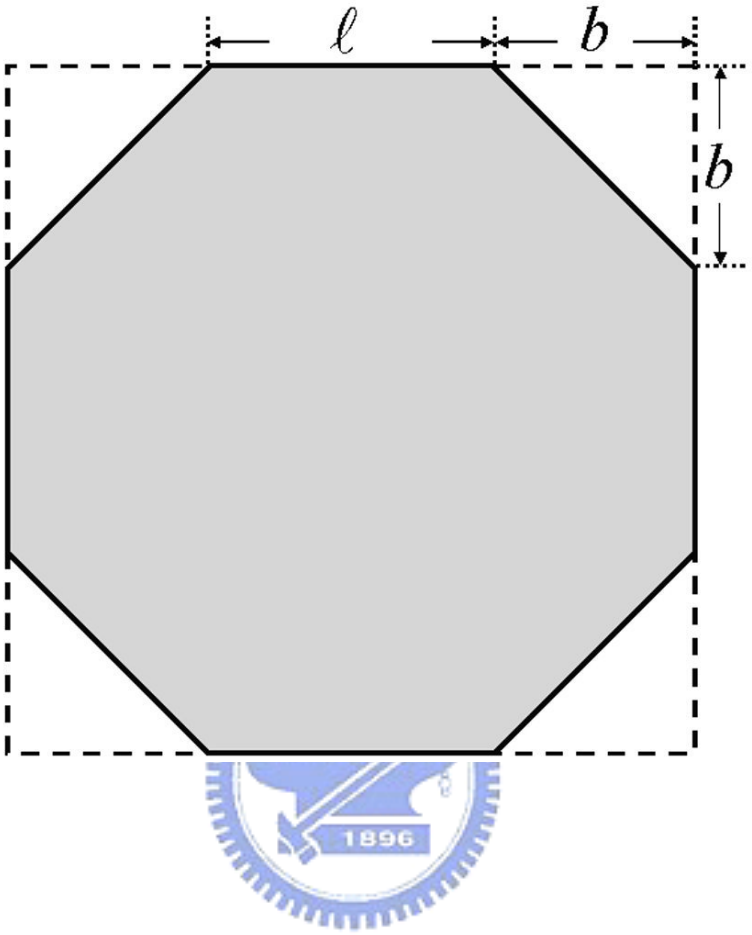

Figure 4.8 The representation and cross-sectional geometry of the rods.

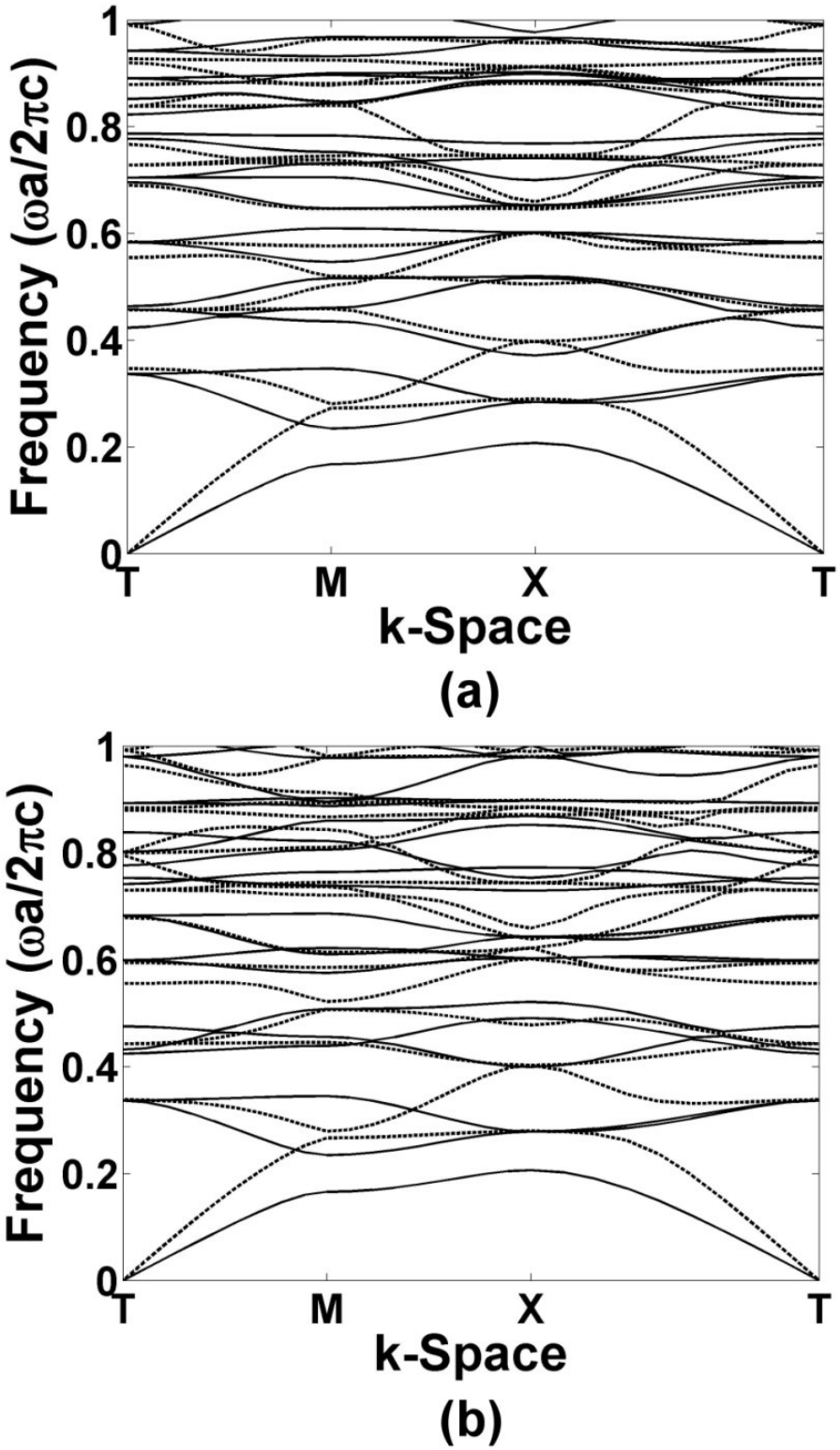

Figure 4.9 Photonic band structures for (a) square rods ($b = 0$) and (b) octagonal rods ($b = 15 \cdot \beta$) in the square lattice, at a filling factor of 0.45.

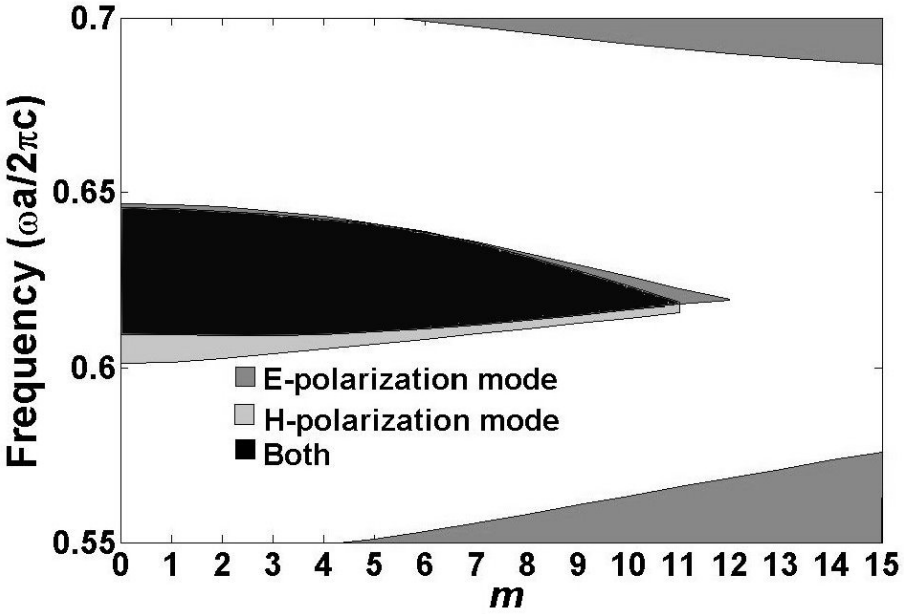

Figure 4.10 The gap map as a function of *m*, and the corresponding size of cutting corner for each structure is $m \cdot \beta$.

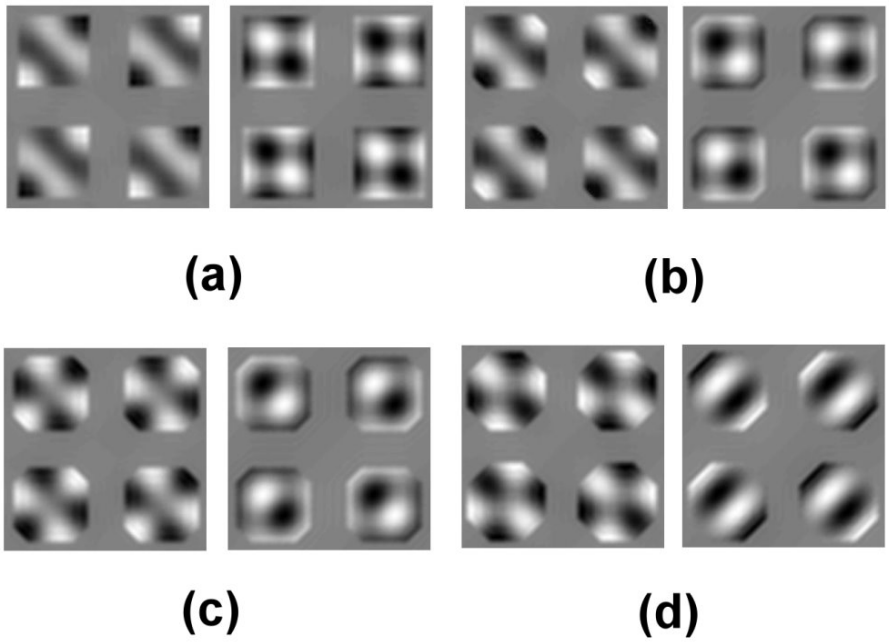

Figure 4.11 Field patterns of E-polarization modes inside the dielectric rods of (a) m=0 (b) m=8 (c) m=10 and (d) m=15, for the E_8 band and at the *M*-symmetry point.

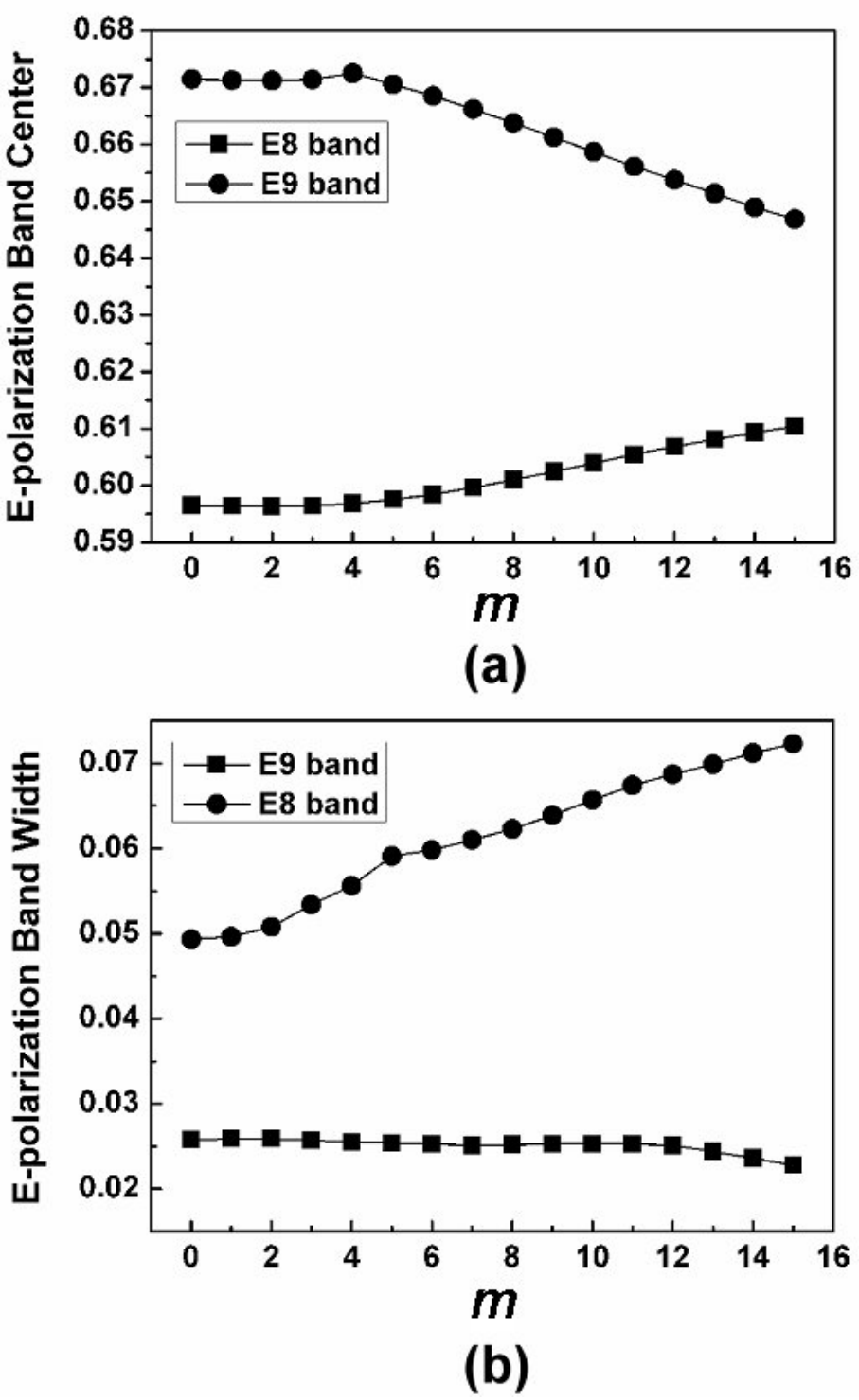

Figure 4.12 The (a) band center and (b) band width associated with E_8 and E_9 bands as a function of m.

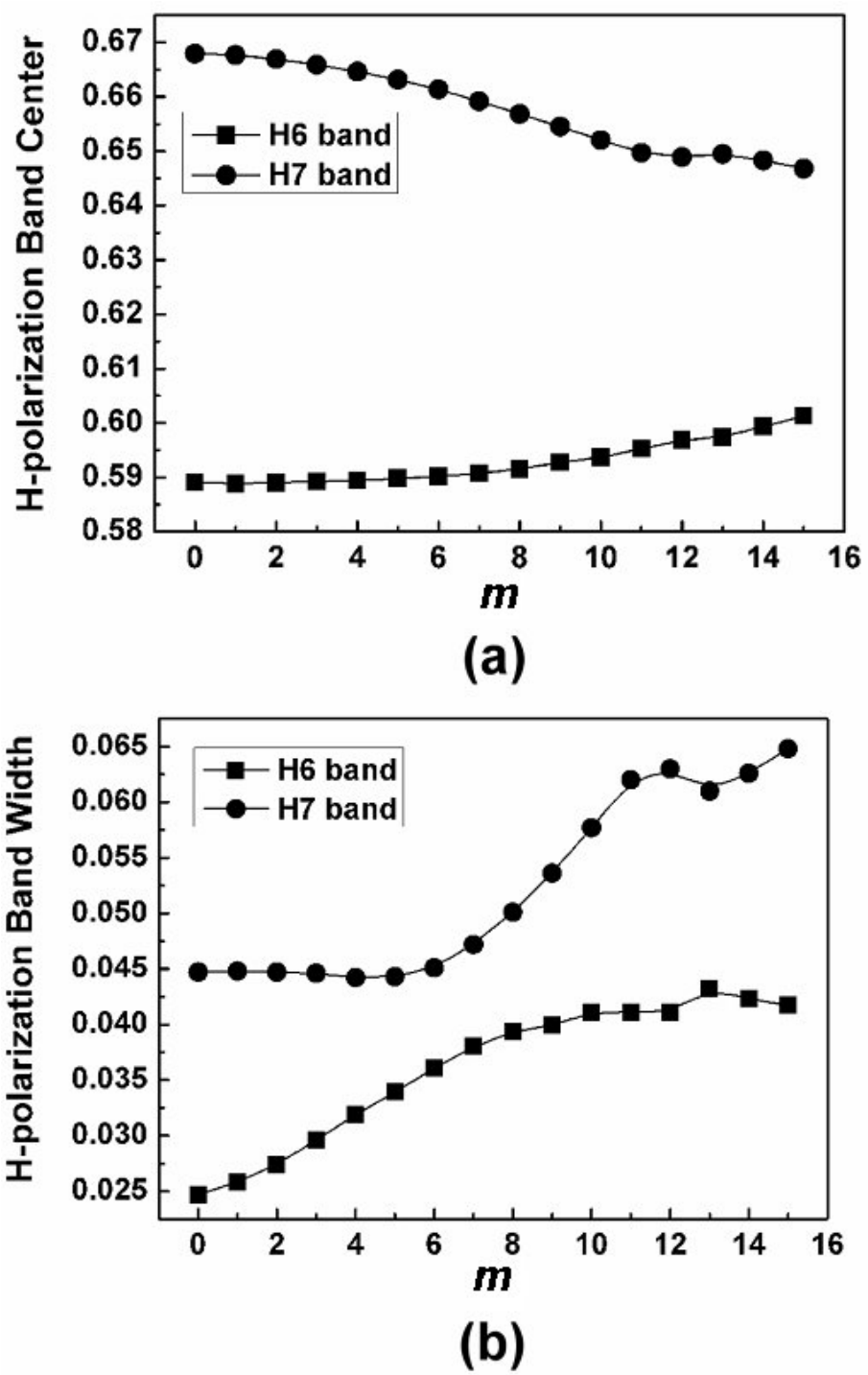

Figure 4.13 (a) Band center and (b) band width associated with H_6 and H_7 bands as a function of m.